Geochemical Journal, Vol. 41, pp. 379 to 389, 2007

Retention of aqueous Ba^{2+} ions by calcite and aragonite over a wide range of concentrations: Characterization of the uptake capacity, and kinetics of sorption and precipitate formation

Ö. TUNUSOĞLU, T. SHAHWAN* and A. E. EROĞLU

Department of Chemistry, Izmir Institute of Technology, Urla 35430, Izmir, Turkey

(*Received November 28, 2006; Accepted July 24, 2007*)

The uptake of aqueous Ba^{2+} ions by abiogenic calcite and aragonite was studied over a wide range of concentration; 1.0×10^1, 5.0×10^1, 1.0×10^2, 5.0×10^2, 1.0×10^3, 5.0×10^3, and 1.0×10^4 mg/L. The uptake process was characterized using ICP-AES, XRPD, SEM/EDS, and FTIR techniques. Up to the initial concentration of 5.0×10^2 mg/L, the uptake of Ba^{2+} ions was fast and obeyed Lagergren's kinetic model. The equilibrium data were adequately described using Freundlich isotherm model. The overgrowth of $BaCO_3$ (witherite) took place at higher concentrations, in a kinetically slow process and enhanced the uptake of Ba^{2+} ions. Quantitative XRPD was used to evaluate the fractions of precipitated $BaCO_3$ on calcite and aragonite minerals and monitor their variation with time. At all the studied concentrations, aragonite showed higher removal capacity of Ba^{2+} and faster uptake kinetics than did calcite. The precipitated crystals appeared to predominantly possess olivary-like morphology with an average particle size of 1–2 μm. EDS was used to reveal the elemental quantities of Ba and Ca after $BaCO_3$ formation on calcite and aragonite surfaces. FTIR spectroscopy was employed to analyze the vibrational modes in carbonate mixtures upon incorporation of Ba^{2+} by sorption and precipitation mechanisms.

Keywords: barium, calcite, aragonite, witherite, XRPD

INTRODUCTION

Calcite and aragonite are two polymorphs of natural $CaCO_3$ which can also exist, to a lesser extent, as vaterite. Even though calcite and aragonite are chemically identical, they exhibit different carbonate group symmetries and as a result their crystal structures are different. Calcite belongs to the rhombohedral crystal system while aragonite is orthorhombic, and the former is thermodynamically more stable. The coordination number for calcite is 6, while for aragonite the coordination number is 9.

Carbonate minerals, which are widely available in soil and rock bodies, possess a dynamic surface in contact with aqueous media. As a result, they are effective in biogeochemical cycling and consequently the dispersion or accumulation of various metals in the environment. The chemical regulation of metals in aquatic environments can broadly take place via precipitation, dissolution, and sorption reactions which are in turn controlled by the chemical processes taking place at the interface between the mineral lattice and the bulk solution (Morse, 1986). Knowledge of the retention capacity and nature of interaction of the metal ions with carbonate minerals is essential for predicting the extent to which these metals can be retarded or dispersed into the environment. The scavenging capacity of calcium carbonate minerals has been investigated for various types of metallic and nonmetallic pollutants (e.g., Cave and Talens-Alesson, 2005; Al-Degs *et al*., 2006; Gómez del Río *et al*., 2004; Shahwan *et al*., 2005, Karageorgiou *et al*., 2007, Román-Ross *et al*., 2006).

Barium, Ba, an alkaline earth element (Z = 56) that lies in the same group with calcium, is conceived as a heavy metal. Compared to other heavy metals, Ba^{2+} ions possess a relatively low hydration energy, the property that yields more mobility in aqueous systems. The compounds of Ba are used in various industries like paint, glass, and pottery (Iucolano *et al*., 2005). Once contained in industrial waste water, Ba^{2+} can potentially spread into environmental cycles, and exposure to high doses can be fatal. This element possesses also a large number of radioactive isotopes, but the most important ones are ^{133}Ba ($t_{1/2}$ = 10.7 y) which has a relatively long half life, and ^{140}Ba ($t_{1/2}$ = 12.79 day) which is a fission product produced in high yield; 6.21% (Lieser, 1995). In addition, Ba is an ideal analogue of Ra as they occur in the same group and possess close ionic radii (Ba^{2+} = 1.34 Å, Ra^{2+} = 1.43 Å) (Erten and Gokturk, 1990; Curti, 1999). Ra,

*Corresponding author (e-mail: talalshahwan@iyte.edu.tr)

Table 1. Measured pH values at different times of contact of Ba^{2+} ion with calcite and aragonite

Mineral	Time of contact	pH measured at different Ba^{2+} concentrations						
		1.0×10^1 mg/L	5.0×10^1 mg/L	1.0×10^2 mg/L	5.0×10^2 mg/L	1.0×10^3 mg/L	5.0×10^3 mg/L	1.0×10^4 mg/L
Calcite	5 min	9.66	9.61	9.54	9.19	9.16	8.86	8.74
	1 h	9.06	8.88	8.96	8.63	8.59	8.52	8.24
	2 h	8.56	8.69	8.65	8.54	8.51	7.99	7.72
	4 h	8.07	8.30	8.28	8.52	8.32	7.82	7.42
	7 h	7.93	8.04	8.21	6.52	7.90	7.24	6.83
	24 h	8.06	8.05	7.95	7.70	7.99	7.61	7.18
	48 h	7.96	7.90	7.98	8.06	7.95	7.52	7.38
Aragonite	5 min	10.04	10.16	9.74	9.60	9.36	8.63	8.41
	1 h	10.03	9.98	9.64	9.24	8.72	8.08	8.38
	2 h	9.64	9.62	9.50	8.98	8.47	7.67	7.64
	4 h	8.98	8.91	8.79	8.26	8.04	7.35	7.45
	7 h	8.51	8.56	8.52	8.09	7.88	7.38	7.31
	24 h	8.53	8.49	8.30	8.05	7.77	7.25	7.24
	48 h	8.48	8.40	8.36	8.07	7.84	7.27	7.11

which has several radioisotopes that are important in radioactive waste considerations, has a high mobility in the Geosphere and thus high accessibility to the food chain. A major factor in Ra behavior is uptake by vegetation, which concentrates Ra more than U and moves Ra from deeper soil to surface soil (Greeman *et al*., 1999). In line with the analogy between Ba and Ra, similar behavior and partition coefficients were reported for the two elements on calcite (Rihs *et al*., 2000). Literature resources indicate a scarcity of works addressing the topic of Ba^{2+} uptake by calcite and aragonite, in particular investigation of the kinetic aspects at the stage of surface precipitation. An earlier study of Ba^{2+} uptake on calcite using Electron Spectroscopy for Chemical Analysis (ESCA) reported that adsorption proceeds relatively slowly and that ion exchange of Ba^{2+}-Ca^{2+} is the prevailing mechanism, within the studied range of concentrations (Bancroft *et al*., 1977). No similar studies are present for Ba^{2+} sorption on aragonite, according to our literature search. There is, however, a number of studies that focused on the mechanistic details of Ba^{2+} interaction with calcite and aragonite during the stage of crystal growth or dissolution for a specific set of experimental conditions (e.g., Reeder, 1996; Terakado and Taniguchi, 2006).

In an earlier study, we reported that the association of $CaCO_3$ (a mixture of calcite and aragonite) with montmorillonite clay enhanced the removal of aqueous Ba^{2+} ions by virtue of surface precipitation of $BaCO_3$ (Shahwan *et al*., 2002). In this study, the uptake of Ba^{2+} by pure phases of calcite and aragonite were investigated in batch experiments over a wide range of concentrations. Inductively Coupled Plasma-Atomic Emission Spectroscopy (ICP-AES) was used to measure Ba^{2+} concentration in the liquid solutions. Surface precipitation of $BaCO_3$ (witherite) at high concentrations was quantified by using X-ray Powder Diffraction (XRPD) after introducing two equations developed for binary mixtures of $BaCO_3$-calcite and $BaCO_3$-aragonite. Scanning Electron Microscopy-Energy Dispersive X-ray Spectroscopy (SEM/EDS) was used to evaluate Ba and Ca quantities and analyze the distribution of precipitated $BaCO_3$ on aragonite and calcite. The changes in the vibrational bands of the carbonates were studied using Fourier Transform-Infrared Spectroscopy (FTIR).

EXPERIMENTAL

Throughout this study the batch method was applied. Calcite used in this study was obtained from Carlo Erba; XRPD characterization showed that the calcite contained minor amounts of aragonite. Aragonite was synthesized in the laboratory. For this purpose, 0.1 M of calcium chloride ($CaCl_2$, Aldrich) and 0.2 M of magnesium chloride hexahydrate ($MgCl_2 \cdot 6H_2O$ Sigma-Aldrich) were prepared in the same volumetric flask. Next, this solution was poured into a 1 liter Erlenmeyer flask and placed into a Multimatics-9S water bath at 60°C. At the same time, 100 milliliters of 1 M sodium carbonate (Na_2CO_3, Aldrich) was prepared. Both of the solutions were stirred and kept in the water bath for about 2 hours for thermal equilibrium. The Na_2CO_3 solution was then added drop-wise to the solution containing $CaCl_2$ and $MgCl_2 \cdot 6H_2O$ using a peristaltic pump at a flow rate of 1.67 ml/min. After addition, the mixture was stirred in the water bath for another 30 minutes. The pH of the mixture was measured as 8.6. Finally, the white precipitate was separated by vacuum filtration, washed using distilled water, and dried at 110°C. The formation of pure aragonite was confirmed by XRPD analysis.

According to SEM images calcite particles showed

indefinite morphology with variable size (5–15 μm), while aragonite possessed rod-like morphology with a crystal size of 5–10 μm.

In each experiment, 25.0 ml aliquots of $Ba(NO_3)_2$ solutions were mixed with 0.25 g samples of calcite or aragonite powders using a thermostat multi-position magnetic stirrer (Selecta, Multimatic 9S). The initial concentrations were 1.0×10^1, 5.0×10^1, 1.0×10^2, 5.0×10^2, 1.0×10^3, 5.0×10^3, and 1.0×10^4 mg/L and the experiments were carried out at ambient temperature and pressure for time periods ranging from 30 minutes up to 3 weeks. At the end of the mixing period, the solid phase was separated from solution by filtration and dried at 60°C. All the experiments were performed in duplicate. Throughout this study no pH adjustment was done. The measured pH values at different periods of contact for the studied concentrations are provided in Table 1. The chemical speciation analysis of aqueous Ba^{2+} ions was performed using visual MINTEQ software. This software has been applied in many studies on metal sorption by soil fractions (e.g., Kaplan and Knox, 2004; Kasama *et al*., 2004). Under different input parameters, up to pH value of about 12, the dominant chemical form of Ba is Ba^{2+}. Beyond this value, the chemical form in aqueous solution will mainly be $BaOH^+$.

A Varian Liberty Series II Axial view ICP-AES was used in the determination of aqueous barium concentration. The instrument was operated with incident power of 1.2 kW, plasma gas flow rate of 15 L/min, and auxiliary gas flow rate of 1.5 L/min. Continuous nebulization was realized by means of a concentric glass nebulizer with cyclonic chamber. The sampling flow rate was 1.0 mL/min. Measurements were based on peak height with polynomial plotted background correction method.

XRPD analysis was performed using a Philips X'Pert Pro instrument. The samples were first ground, mounted on holders then introduced for analysis. The source consisted of Cu K_α radiation (λ = 1.54 Å). Each sample was scanned within the 2 theta range of 15–60.

SEM/EDS characterization was carried out using a Philips XL-30S FEG type instrument. Prior to analysis, the solid samples were sprinkled onto adhesive aluminum tapes supported on metallic disks. Images of the sample surfaces were then recorded at different magnifications. Elemental EDS analysis was performed at randomly selected areas on the solid surfaces each being approximately 100 μm × 100 μm in dimension.

FTIR spectra of the samples were collected in the middle IR region, 400–4000 cm^{-1}, using a Nicolet Magna 550 type instrument. After mixing with KBr, the samples were introduced as pellets and KBr powder was used as a reference spectrum. A total of 32 scans were recorded with a resolution of 4 cm^{-1} for each spectrum. Omnic 1.3 software was used to process the results.

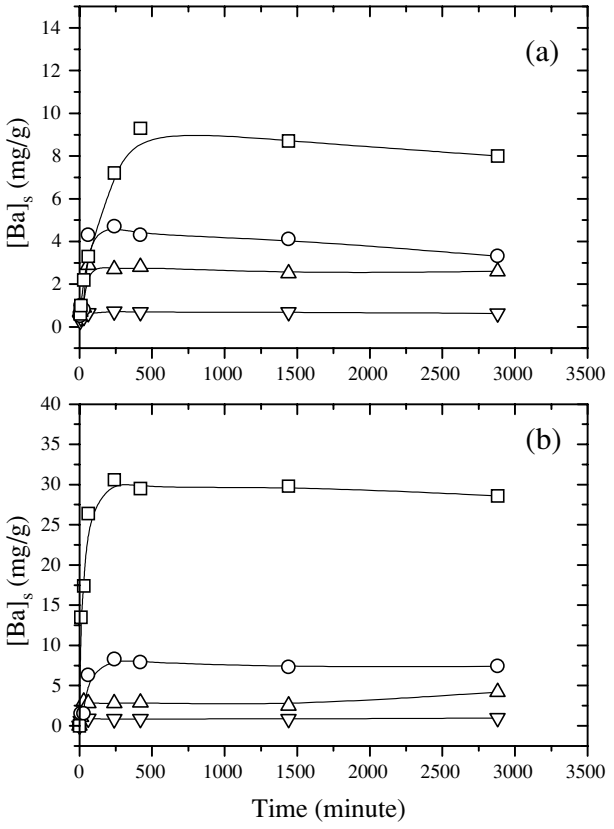

Fig. 1. The amount of Ba^{2+} (mg/g) adsorbed as a function of time on: (a) calcite, (b) aragonite. Initial Ba^{2+} concentrations are: ▽: 1.0×10^1 mg/L, △: 5.0×10^1 mg/L, ○: 1.0×10^2 mg/L, □: 5.0×10^2 mg/L.

Results and Discussion

The uptake of Ba^{2+} by calcite and aragonite was studied over the initial concentration range 1.0×10^1, 5.0×10^1, 1.0×10^2, 5.0×10^2, 1.0×10^3, 5.0×10^3, and 1.0×10^4 mg/L. XRPD analysis revealed that precipitate formation of $BaCO_3$ started at the initial Ba^{2+} concentration 1.0×10^3 mg/L in the case of calcite, whereas in the case of aragonite, some $BaCO_3$ overgrowth was observed at the initial concentration of 5.0×10^2 mg/L. Up to the initial concentration of 1.0×10^3 mg/L, Ba^{2+} cations were fixed by calcite and aragonite via a kinetically fast sorption process. Here the term "sorption" is loosely used to stand for all possible fixation mechanisms other than precipitate formation.

The variation of the adsorbed Ba^{2+} amount on calcite and aragonite with time in the concentration range 1.0×10^1–5.0×10^2 mg/L is demonstrated on Fig. 1. The figure shows that the time required to approach equilibrium increases with the increase in initial concentration, with a time period of about 10 hours being sufficient to reach

Table 2. The values of the distribution ratio, R_d, and the percentage uptake of Ba^{2+} ions on calcite and aragonite when equilibrium is achieved

Mineral	$[C]_o$ (mg/L)	$[C]_l$ (mg/L)	$[C]_s$ (mg/g)	$R_d = [C]_s/[C]_l$ (L/g)	% Uptake
Calcite	1.0×10^1	3.7	0.63	0.17	63
	5.0×10^1	24	2.5	0.11	52
	1.0×10^2	67	3.3	0.05	33
	5.0×10^2	420	8	0.02	16
Aragonite	1.0×10^1	0.3	0.97	3.2	97
	5.0×10^1	8	4.2	0.53	84
	1.0×10^2	26	7.4	0.28	74
	5.0×10^2	241	28.6	0.12	52

equilibrium at the highest initial concentration, i.e., 5.0×10^2 mg/L. At all concentrations and contact times, more Ba^{2+} is removed by aragonite in comparison with calcite. Based on a thermodynamic model by Wang and Xu (2001), a larger partition coefficient of Ba^{2+} in aragonite compared to calcite was predicted. The values of the distribution ratio, R_d, and the percentage uptake of Ba^{2+} ions on both minerals when equilibrium is achieved are given in Table 2.

The kinetic data corresponding to the Ba^{2+} initial concentration of 5.0×10^2 mg/L, which showed the largest variation with time were fitted using various kinetic models. The kinetic description was first attempted by focusing on the removal of Ba^{2+} ions from the aqueous medium (rather than their uptake by the solid minerals) through the application of the conventional first order, $\ln([Ba]_l/[Ba]_o) = -k_1 t$, and second order, $1/[Ba]_l = k_2 t + 1/[Ba]_o$, integrated rate equations. Both of these equations that are given in terms of the initial and equilibrium liquid concentrations did not provide statistically significant correlations with the experimental data. Alternatively, Lagergren's equation was found to properly describe the kinetic data corresponding to the pre-saturation region. This equation was originally derived under pseudo approximation for first order kinetics and expressed in terms of the concentration of the sorbate on the solid phase using:

$$\ln\left(1 - \frac{[C]_s}{C_m}\right) = -kt \qquad (1)$$

where $[C]_s$ is the concentration of sorbed ion on the solid at time t (mg/g), C_m is the concentration of sorbed ion at equilibrium, k is the rate constant (min^{-1}). The obtained linear fits are shown in Fig. 2. The rate constants were obtained as 6.4×10^{-3} and 1.6×10^{-2} min^{-1} for Ba^{2+} uptake by calcite and aragonite, respectively. This indicates that Ba^{2+} is retained faster by aragonite compared to calcite.

The data corresponding to the equilibrium conditions within the sorption range, 1.0×10^1–5.0×10^2 mg/L initial Ba^{2+} concentration, were used to check the best fitting adsorption isotherm. The results were most adequately described by Freundlich isotherm model, the linear form of which is given by the equation:

$$\log[C]_s = \log k + n \log[C]_l. \qquad (2)$$

Here $[C]_s$ stands for the equilibrium concentration of Ba^{2+} on the solid (mg/g), while $[C]_l$ is the equilibrium concentration of Ba^{2+} in solution (mg/L). In both cases, the data corresponding to a contact time of 48 hours were used. Freundlich constants k and n can be used, respectively, to estimate adsorption affinity and linearity. According to the linear fits of the data shown in Fig. 3, the values of k for the adsorption of Ba^{2+} on calcite and aragonite were 0.37 and 1.62, respectively. These values confirm that Ba^{2+} is more preferably adsorbed by aragonite. On the other hand, the values of n were 0.52 and 0.50 for Ba^{2+} adsorption by calcite and aragonite, respectively. This shows that adsorption proceeds nonlinearly and that, as Ba^{2+} loading is increased, the extent of increase in the energy barrier of uptake is approximately the same for both of calcite and aragonite.

In general, the uptake mechanism on calcium carbonate is strongly pH dependent and can plausibly occur via various processes; ion exchange with Ca^{2+} ions located on the mineral surface, burial of the ions within the lattice of carbonate upon recrystallization, formation of surface complexes with >CaOH and $>CO_3H$ groups, coprecipitation, precipitation as metal-carbonate, metal hydroxide, or both, and solid state diffusion (Xu *et al.*, 1996).

When the solution is under-saturated with respect to $BaCO_3$ formation, Ba^{2+} ions might be fixed primarily by the surface groups on calcite and aragonite via surface complexation. Since the size of Ba^{2+} (1.36 Å) consider-

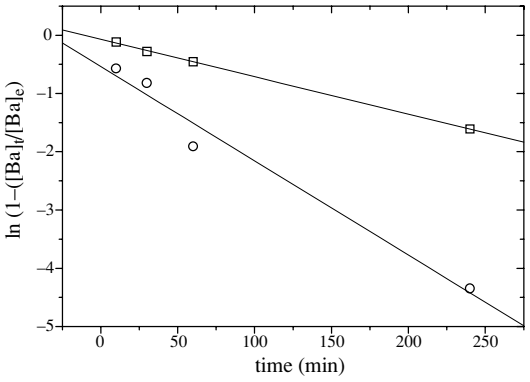

Fig. 2. Lagergren's fits of the experimental data corresponding to Ba^{2+} initial concentration of 5.0×10^2 mg/L. □: Ba-calcite, ○: Ba-aragonite.

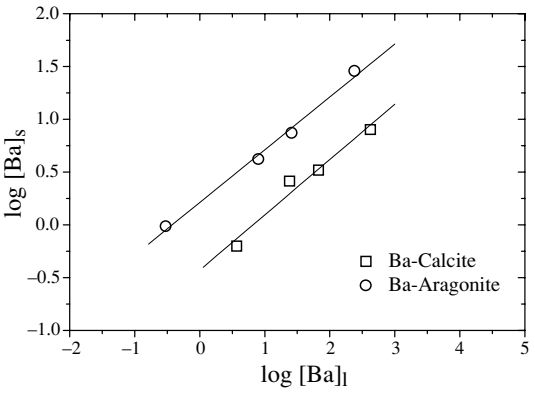

Fig. 3. Freundlich isotherm plot of the equilibrium adsorption data of Ba^{2+} on calcite and aragonite. The linear correlation coefficients are 0.9829 and 0.9963, respectively.

ably exceeds that of Ca^{2+} (0.99 Å), the contribution of the ion exchange and coprecipitation mechanisms to the uptake of Ba^{2+} by calcite and aragonite is expected to be small. Low partition coefficients for Ba^{2+}, in comparison to ions of similar size to Ca^{2+}, on calcite and aragonite have been reported (Wang and Xu, 2001). As was shown in the speciation analysis, within the pH range of our experiments, the dominating chemical form of barium is Ba^{2+}. The mechanistic details of the sorption of this species on calcite or aragonite are also closely related with surface speciation of these minerals under the operating conditions. It is reported that the cationic species Ca^{2+}, $CaHCO_3^-$, and $CaOH^+$ are dominant when the pH is below 8. Beyond this pH value, negative species prevail but the concentration of the positive species might still be considerable (Karageorgiou *et al*., 2007). In another study (Cappellen *et al*., 1993) about surface complexation on carbonate minerals it was proposed that in the absence of CO_2(g) and away from equilibrium, the surface speciation of calcite is dominated by the reactions:

$$>CO_3H^o \Leftrightarrow >CO_3^- + H^+ \qquad \log K^s_{int} = -4.9$$

$$>CaOH_2^+ \Leftrightarrow >CaOH^o + H^+ \qquad \log K^s_{int} = -12.2$$

$$>CaOH^o \Leftrightarrow >CaO^- + H^+ \qquad \log K^s_{int} = -17.$$

According to the predictions by the given surface complexation model (Cappellen *et al*., 1993), in the pH range 5.5–8, the surface is made up of nearly equal amounts of $>CaOH_2^+$ and $>CO_3^-$ sites. As the pH value is raised beyond 9, a decrease in the abundance of $>CaOH_2^+$ occurs with a progressive increase in the amount of $>CaOH^o$ sites. Experimental evidence based on XPS findings indicated also that hydration of the calcite surface leads to the formation of $>CaOH^o$ and $>CO_3H^o$ (Stipp and Hochella, 1991; Xu *et al*., 1996). With the above in mind, when the solution is undersaturated with respect to $BaCO_3$ formation and within the pH range of our experiments, the fixation of Ba^{2+} ions might be expected to take place primarily through the complexation reactions:

$$>CO_3H^o + Ba^{2+} \Leftrightarrow >CO_3Ba^+ + H^+$$

$$>CaOH^o + Ba^{2+} \Leftrightarrow >CaOBa^+ + H^+.$$

Those reactions are merely suggested ones and lack confirmation using surface sensitive techniques.

Moreover, within the pH conditions of this study, the speciation of $CaCO_3$ suggests that the bicarbonate species concentration is larger than that of carbonate species. Bicarbonates are reported to play a central role in the adsorption and surface precipitation of metal ions on calcite (Zhu, 2002). Applying the reported model to the case of Ba^{2+}, the following reactions can be proposed for adsorption and precipitation of calcite:

$$>CaCO_3^o + Ba^{2+} + HCO_3^- \Leftrightarrow CaCO_3(s) + >BaCO_3^o + H^+$$

$$>BaCO_3^o + Ba^{2+} + HCO_3^- \Leftrightarrow BaCO_3(s) + >BaCO_3^o + H^+$$

where the ">" sign refers to species bound to the surface while (s) is used to denote metal carbonate formation in the bulk of the solution followed by precipitation onto the mineral surface, a process expected to take place at the conditions of supersaturation. At the initial Ba^{2+} concentration of 1.0×10^3 mg/L, a small amount of $BaCO_3$ precipitate formation took place upon interaction with calcite, but comparatively a larger amount resulted from the interaction of Ba^{2+} with aragonite. The extent of $BaCO_3$ overgrowth increased with the increasing initial concentration of Ba^{2+}, and the attainment of equilibrium

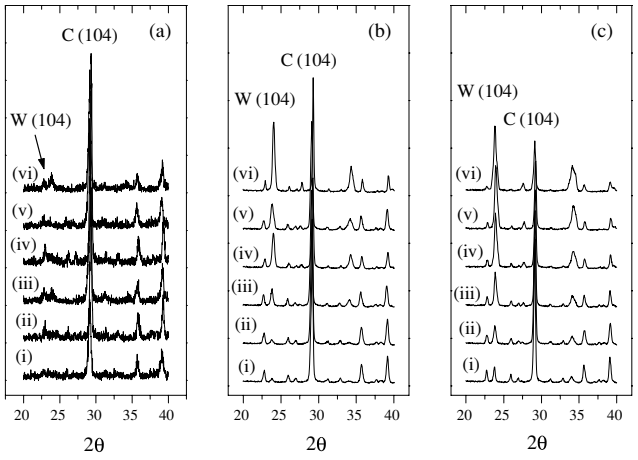

Fig. 4. XRPD patterns showing the overgrowth of $BaCO_3$ (104) reflection on calcite at the initial Ba^{2+} concentrations of; (a) 1.0×10^3 mg/L, (b) 5.0×10^3 mg/L, and (c) 1.0×10^4 mg/L. (i) 30 minutes, (ii) 2 hours, (iii) 7 hours, (iv) 24 hours, (v) 1 week, (vi) 3 weeks.

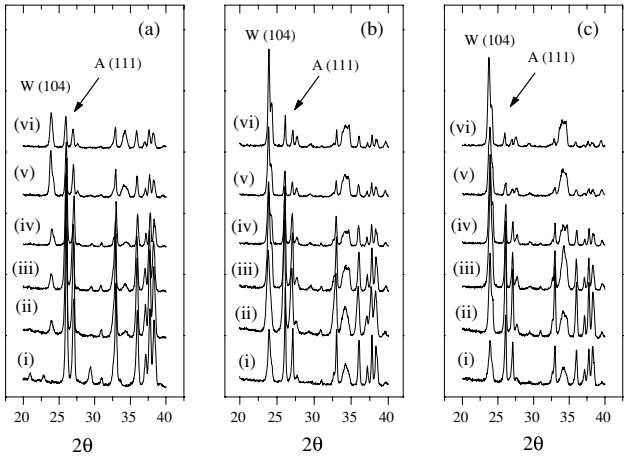

Fig. 5. XRPD patterns showing the overgrowth of $BaCO_3$ (104) reflection on aragonite at the initial Ba^{2+} concentrations of; (a) 1.0×10^3 mg/L, (b) 5.0×10^3 mg/L, and (c) 1.0×10^4 mg/L. (i) 30 minutes, (ii) 2 hours, (iii) 7 hours, (iv) 24 hours, (v) 1 week, (vi) 3 weeks.

was much slower than with lower concentrations. The process was examined over a time period ranging from 30 minutes up to 3 weeks, during which the samples were kept closed to the atmosphere. XRPD patterns that reveal the overgrowth of $BaCO_3$ formation at different times on calcite and aragonite for the initial Ba^{2+} concentrations of 1.0×10^3, 5.0×10^3, and 1.0×10^4 mg/L are shown in Figs. 4 and 5 for both of calcite and aragonite cases. These concentrations are much higher than the encountered ordinary levels of concentration, and are applied in order to quantitatively follow the overgrowth of $BaCO_3$ over a wide range of time. Unfortunately, ICP-AES measurements did not yield results reliable enough to quantify the uptake processes at higher initial Ba^{2+} concentration. The high solution concentration necessitated large dilution factors and consequently resulted in considerable associated uncertainty. Therefore, quantitative XRPD was applied to follow the uptake of Ba^{2+} in the form of $BaCO_3$ at those concentrations.

In an XRPD diagram, the intensity of X-rays reflected by a component is directly proportional to the quantity of that component, inversely proportional to the mass absorption coefficient of the mixture, and can be also dependent on any particular reflection line under consideration (Ouhadi and Yong, 2003). For the purpose of XRPD quantification, first a calibration curve was constructed by recording the XRPD patterns of artificial $BaCO_3$-calcite and $BaCO_3$-aragonite mixtures using the pure phases of the three minerals. These mixtures were prepared such that the mass fraction of $BaCO_3$ is 0.10, 0.20, 0.30, 0.40, 0.50, 0.60, 0.70, 0.80, and 0.90, with the remaining mass fractions corresponding to pure calcite or aragonite. From the obtained multiple XRPD patterns, the peak areas of the basic 104 reflections of $BaCO_3$, calcite and 111 reflection of aragonite were calculated by integration utilizing Origin 5.0 software. The ratios of $BaCO_3$/calcite and $BaCO_3$/aragonite were then calculated and plotted against the mass fraction of $BaCO_3$. Finally, the obtained data were fitted using MS Excel to mathematical equations that enable calculation of the fraction of $BaCO_3$ in any binary mixture with calcite or aragonite from the areas of the XRPD basic reflections. In doing this quantification process it is implicitly assumed that the mass absorption coefficient of the artificial binary mixtures mentioned above is identical to that of the mixtures resulting after surface precipitation of $BaCO_3$ on calcite or aragonite. Moreover, the intensity of each of the major reflection lines; 104 for calcite and $BaCO_3$, and 111 for aragonite, is affected by the crystallinity of the corresponding carbonate phase. Each of these major reflections is considered to be representative enough for its corresponding metal carbonate, i.e., there is no need to consider all reflections in each diffraction pattern.

According to the obtained results, for a binary mixture of $BaCO_3$ and calcite, the fraction of the former can be calculated using the equation:

$$X_W = \frac{0.61\left(I_W / I_C\right)}{1 + 0.52\left(I_W / I_C\right)}. \qquad (3)$$

Here, X_W corresponds to the mass fraction of $BaCO_3$ (witherite), I_W and I_C are, respectively, the integrated intensity of 104 reflection of $BaCO_3$ and calcite.

Alternatively, in a binary mixture of $BaCO_3$ and aragonite, the fraction of $BaCO_3$ can be obtained using the equation:

$$X_W = \frac{0.28(I_W / I_A)}{1 + 0.19(I_W / I_A)} \quad (4)$$

where I_A refers to the integrated intensity of aragonite 111 reflection. The standard deviations associated with the fits of Eqs. (3) and (4) were 3.3% and 1.8%, respectively.

Equations (3) and (4) were used to calculate the fraction of precipitated $BaCO_3$ upon contact of Ba^{2+} solutions with calcite and aragonite at different contact times. The variation of the fraction of $BaCO_3$ as a function of time for the initial Ba^{2+} concentrations of 5.0×10^3 and 1.0×10^4 mg/L are plotted in Fig. 6 for calcite and arago-

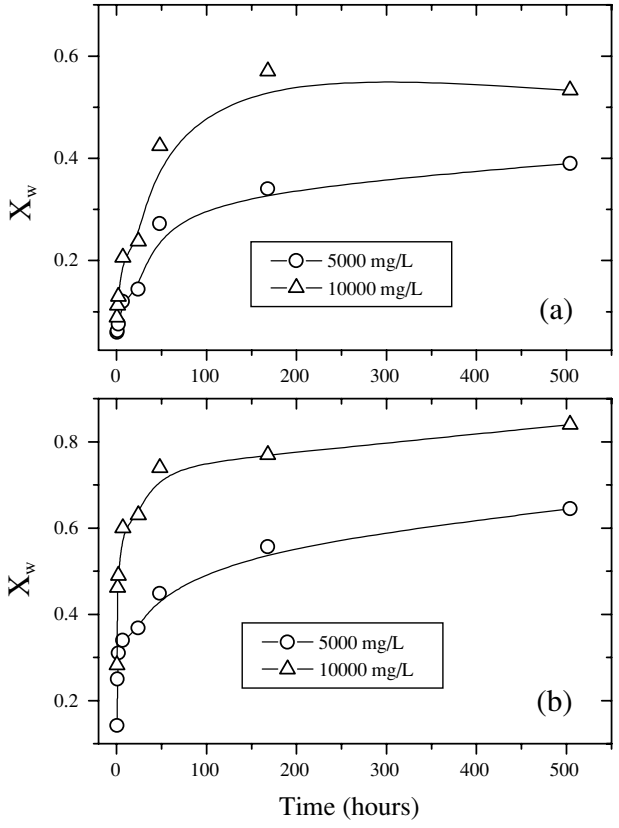

Fig. 6. Variation of precipitated $BaCO_3$ (witherite) fraction, X_w, as a function of time for the uptake of Ba^{2+} on: (a) calcite, (b) aragonite.

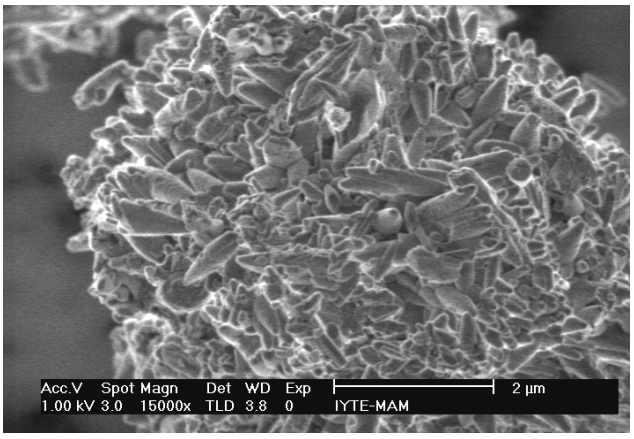

(a)

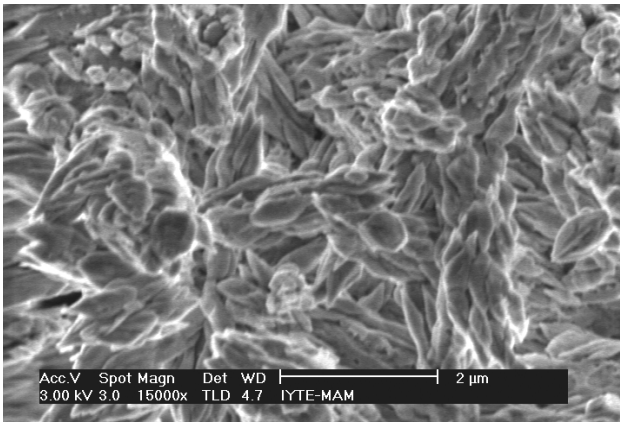

(b)

Fig. 7. SEM microimages showing the particle morphology (olivary-like) of $BaCO_3$ precipitated on: (a) calcite, (b) aragonite.

Table 3. Mass and atomic ratios of Ba/Ca in calcite and aragonite sample after the precipitation of $BaCO_3$. The contact time is 3 weeks, and all data are based on EDS measurements.

Ratio	Initial Ba^{2+} concentration is 1.0×10^3 mg/L		Initial Ba^{2+} concentration is 5.0×10^3 mg/L		Initial Ba^{2+} concentration is 1.0×10^4 mg/L	
	$BaCO_3$-calcite	$BaCO_3$-aragonite	$BaCO_3$-calcite	$BaCO_3$-aragonite	$BaCO_3$-calcite	$BaCO_3$-aragonite
Ba/Ca (mass)	0.14	0.32	1.38	1.88	1.58	3.33
Ba/Ca (atomic)	0.039	0.095	0.40	0.53	0.47	0.96

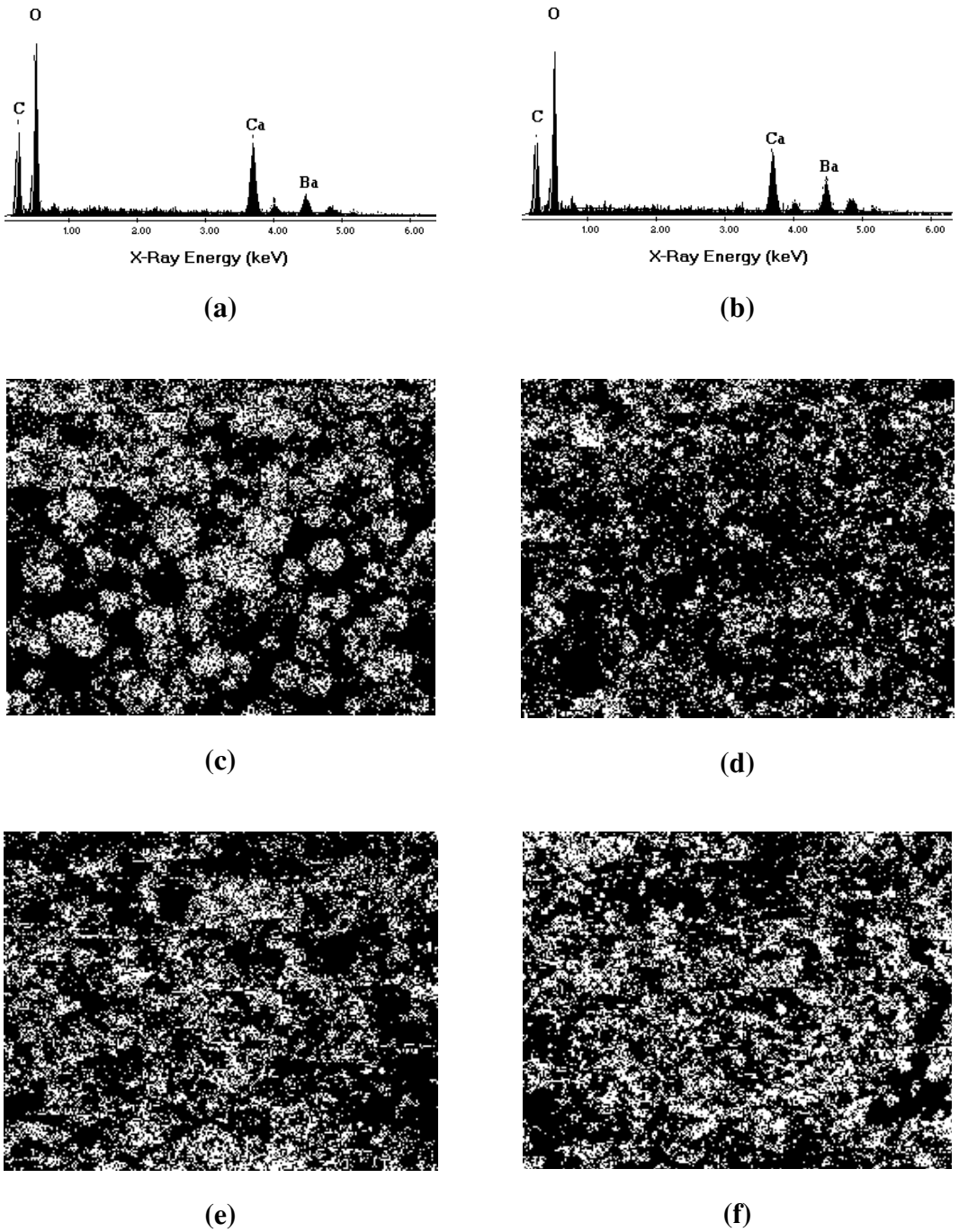

Fig. 8. (a) A typical EDS spectrum of $BaCO_3$-calcite after a 3 week period of interaction at Ba^{2+} initial concentration of 1.0×10^4 mg/L. (b) A typical EDS spectrum of $BaCO_3$-aragonite after a 3 week period of interaction at Ba^{2+} initial concentration of 1.0×10^4 mg/L. (c) X-ray map showing the distribution of Ca on $BaCO_3$-calcite surface. (d) X-ray map showing the distribution of Ba on $BaCO_3$-calcite surface. (e) X-ray map showing the distribution of Ca on $BaCO_3$-aragonite surface. (f) X-ray map showing the distribution of Ca on $BaCO_3$-aragonite surface.

nite cases. The curves indicate the importance of the time factor in the extent of $BaCO_3$ overgrowth on both carbonates, where about one week is required to start approaching equilibrium. The precipitation mechanisms enhanced largely the removal of Ba^{2+} ions in comparison with other possible mechanisms operating at low concentrations. Comparatively, larger amounts of $BaCO_3$ are formed upon uptake of Ba^{2+} by aragonite, and the pre-

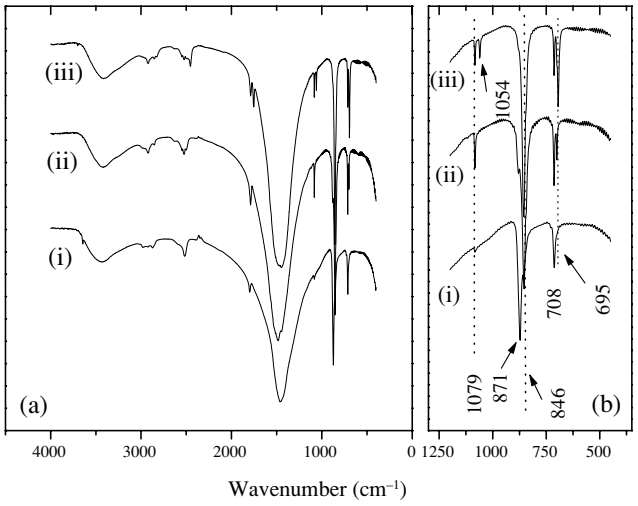

Fig. 9. FTIR spectra of: (i) calcite, (ii) Ba-calcite following the sorption of Ba^{2+} at 5.0×10^2 mg/L initial concentration, and (c) $BaCO_3$-calcite resulting from the uptake of Ba^{2+} at 1.0×10^4 mg/L initial concentration.

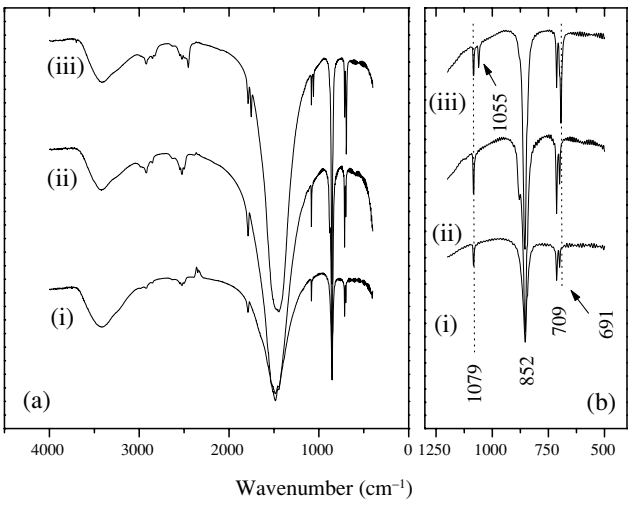

Fig. 10. FTIR spectra of: (i) aragonite, (ii) Ba-aragonite following the sorption of Ba^{2+} at 5.0×10^2 mg/L initial concentration, and (c) $BaCO_3$-aragonite resulting from the uptake of Ba^{2+} at 1.0×10^4 mg/L initial concentration.

cipitate overgrowth on the same mineral occurs at a faster rate, which is in line with the results obtained for lower Ba^{2+} initial concentrations. The fact that $BaCO_3$ possesses an orthorhombic crystal structure, as it is the case with aragonite, is probably responsible for this result. Cations larger in size than Ca^{2+} (0.99 Å) like Ba^{2+} (1.36 Å) and Sr^{2+} (1.16 Å) are generally known to form less stable carbonate minerals with a calcite structure. A calcite-like structure with its six-fold coordination is less suitable for incorporating a large cation like Ba^{2+} in comparison to the nine-fold sites of an aragonite-like structure.

SEM images of the mineral surfaces showed that $BaCO_3$ was dominated by particles showing olivary-like morphology that are about 1–2 μm in size. Typical SEM images obtained for precipitated $BaCO_3$ on calcite and aragonite are presented in Fig. 7.

EDS was used to evaluate the elemental composition of calcite and aragonite samples after the overgrowth precipitation of $BaCO_3$. This analysis included the samples obtained after a contact time of three weeks, with Ba^{2+} initial concentration being 1.0×10^3, 5.0×10^3, and 1.0×10^4 mg/L. Below those concentrations, Ba signals were barely detected by this technique. The EDS spectra were recorded from several randomly selected regions per sample with approximate dimensions of 100 μm × 100 μm for each region. The averaged mass and atomic ratios of Ba/Ca in each of the analyzed samples are provided in Table 3. Typical EDS spectra corresponding to $BaCO_3$-calcite and $BaCO_3$-aragonite are presented in Figs. 8(a) and (b). The results show the extent of increase in Ba quantities as the initial concentration is increased, and confirm the previous results that showed aragonite as a more favorable sink for Ba^{2+} ions.

The distribution of Ba^{2+} in the carbonate surface in comparison to that of Ca^{2+} was characterized using EDS mapping. X-ray maps were recorded over areas of approximate dimensions of 100 μm × 100 μm. These maps contain elemental signals obtained upon interaction of the primary electron beam of the source with atoms in the sample, causing shell transitions in these atoms and subsequent characteristic X-ray emission. Typical maps of Ca (K-line) and Ba (L-line) obtained from $BaCO_3$ precipitate on calcite and aragonite are given in Figs. 8(c), (d) and (e), (f), respectively. In the $BaCO_3$-calcite sample, the Ca-rich cores appear to include large spheroidal grains that are surrounded by more finely distributed Ba-containing phase (presumably $BaCO_3$). In $BaCO_3$-aragonite case, more intense Ba maps were obtained. Compared with $BaCO_3$-calcite samples, the exterior rims of the carbonate grains are less distinguishable and appear more uniformly distributed. However, closer inspection reveals the presence of Ba- and Ca-rich regions corresponding to the two distinct carbonate phases.

FTIR spectroscopy was employed to analyze the vibrational modes in carbonate mixtures upon incorporation of Ba^{2+} by sorption and precipitation mechanisms. It is well known that the vibrational spectra of carbonate minerals contain modes caused by symmetric stretching ($\nu 1$), out-of-plane bending ($\nu 2$), asymmetric stretching ($\nu 3$), in-plane-bending ($\nu 4$), in addition to the two combination modes ($\nu 1 + \nu 3$) and ($\nu 1 + \nu 4$). As shown in Fig. 9(i), in pure calcite, the bands of $\nu 2$, $\nu 3$, $\nu 4$ appeared to be centered at 871, 1447, and 708 cm^{-1}, respectively. The band corresponding to the vibrational mode $\nu 1$, which

theoretically is IR inactive in calcite, was very weak and centered at 1079 cm^{-1}, and is attributed to the presence of a small quantity of aragonite in the calcite structure, as was mentioned previously. On the other hand, the FTIR bands of pure aragonite applied in this work, $\nu 1$, $\nu 2$, $\nu 3$, and $\nu 4$, were centered at 1079, 852, 1477, and 709 cm^{-1}, respectively as shown in Fig. 10(i). In both cases, the uptake of aqueous Ba^{2+} ions via a sorption mechanism (when no surface precipitation is observed) have resulted in an increase of the $\nu 1$ intensity, and significant splits in the bands of $\nu 2$ and $\nu 4$ towards lower wavenumbers. Changes in the vibrational bands are consequences of the variations in the molecular environment of carbonate groups in calcite and aragonite and suggest that the uptake of Ba^{2+} lead to shifting the vibrational energies of carbonate group towards lower values. Such changes were enhanced further by the increase in the concentration of Ba^{2+} ions. The FTIR spectra of calcite and aragonite after interaction with 5.0×10^2 mg/L Ba^{2+} solution are, respectively, given in Figs. 9(ii) and 10(ii).

When $BaCO_3$ appeared as a distinct phase as a result of precipitation at concentrations beyond 1.0×10^3 mg/L, a split in the $\nu 1$ band took place and the splits in $\nu 2$ and $\nu 4$ modes were greatly enhanced for both of calcite and aragonite cases. All the splits occurred at lower wavenumbers. FTIR spectra of calcite and aragonite loaded with 1.0×10^4 mg/L Ba^{2+} initial concentration are shown in Figs. 9(iii) and 10(iii), respectively. The emerging features were assigned to $BaCO_3$ fractions in the carbonate mixtures. To confirm this assignment, FTIR spectra of a separate pure sample of $BaCO_3$ were recorded and compared. According to the results, the bands of $\nu 1$, $\nu 2$, $\nu 3$, $\nu 4$ in pure $BaCO_3$ occur at 1056, 854, 1432, and 690 cm^{-1}, respectively, which are very close to the newly emerging peaks after precipitation of $BaCO_3$ on calcite and aragonite.

Conclusions

Compared to calcite, aragonite was observed to form a more favorable sink for aqueous Ba^{2+} ions, with the uptake process occurring at a faster rate. At lower concentrations, the equilibrium data were adequately described by Freundlich isotherms. Beyond the initial concentration of 1.0×10^3 mg/L, the overgrowth of witherite took place in a kinetically slower process, and quantitative XRPD seemed to serve well in determining the extent of witherite overgrowth at different contact times. The morphology of precipitated witherite crystals was dominated by olivary-like shape, with an average particle size of 1–2 μm. EDS mapping revealed a more intense and uniform distribution of witherite and aragonite grains compared to the case of witherite and calcite. The FTIR bands of calcite and aragonite showed various changes as a result of Ba^{2+} incorporation by sorption or precipitation.

Acknowledgments—The authors acknowledge TUBITAK for the financial support (Project No. 104T089). The authors would like to thank the research specialists Sinan Yılmaz and Oya Altungöz for the help in ICP-AES measurements, Dr. Durmuş Özdemir for his help in the mathematical curve fitting calculations, and the Center of Material Research at Izmir Institute of Technology for the assistance in the SEM and XRPD measurements.

References

Al-Degs, Y. S., El-Barghouthi, M. I., Issa, A. A., Khraisheh, M. A. and Walker, G. M. (2006) Sorption of Zn(II), Pb(II), and Co(II) using natural sorbents: Equilibrium and kinetic studies. *Water Res.* **40**, 2645–2658.

Bancroft, G. M., Brown, J. R. and Fyfe, W. S. (1977) Quantitative X-ray photoelectron spectroscopy (ESCA): Studies of Ba^{2+} sorption on calcite. *Chem. Geol.* **19**, 131–144.

Cappellen, P. V., Charlet, L., Stumm, W. and Wersin, P. (1993) A surface complexation model of the carbonate mineral-aqueous solution interface. *Geochim. Cosmochim. Acta* **57**, 3505–3518.

Cave, K. and Talens-Alesson, F. I. (2005) Comparative effect of Mn(II) and Fe(III) as activators and inhibitors of the adsorption of other heavy metals on calcite. *Colloids and Surfaces A* **268**, 19–23.

Curti, E. (1999) Coprecipitation of radionuclides with calcite: estimation of partition coefficients based on a review of laboratory investigations and geochemical data. *Appl. Geochem.* **14**, 433–445.

Erten, H. N. and Gokturk, H. (1990) Sorption-desorption behavior of barium on clays. *J. Environ. Radioactivity* **11**, 183–188.

Gómez del Río, J. A., Morando, P. J. and Cicerone, D. S. (2004) Natural materials for treatment of industrial effluents: comparative study of the retention of Cd, Zn and Co by calcite and hydroxyapatite. Part I: batch experiments. *J. Environ. Management* **71**, 169–177.

Greeman, D. J., Rose, A. W., Washington, J. W., Dobos, R. R. and Ciolkosz, E. J. (1999) Geochemistry of radium in soils of the Eastern United States. *Appl. Geochem.* **14**, 365–385.

Iucolano, F., Caputo, D. and Colella, C. (2005) Permanent and safe storage of Ba^{2+} in hardened phillipsite-rich tuff/cement pastes. *Appl. Clay Sci.* **28**, 167–173.

Kaplan, D. I. and Knox, A. S. (2004) Enhanced contaminant desorption induced by phosphate mineral additions to sediment. *Environ. Sci. Technol.* **38**, 3153–3160.

Karageorgiou, K., Paschalis, M. and Anastassakis G. N. (2007) Removal of phosphate species from solution by adsorption onto calcite used as natural adsorbent. *Journal of Hazardous Materials* **139**, 447–452.

Kasama, T., Watanabe, Y., Yamada, H. and Murakami, T. (2004) Sorption of phosphates on Al-pillared smectites and mica at acidic to neutral pH. *Appl. Clay Sci.* **25**, 167–177.

Lieser, K. H. (1995) Radionuclides in the Geosphere: sources,

mobility, reactions in natural waters and interactions with solids. *Radiochimica Acta* **70**, 355–375.

Morse, J. W. (1986) The surface chemistry of calcium carbonate minerals in natural waters: An overview. *Mar. Chem.* **20**, 91–112.

Ouhadi, V. R. and Yong, R. N. (2003) Impact of clay microstructure and mass absorption coefficient on the quantitative mineral identification by XRD analysis. *Appl. Clay Sci.* **23**, 141–148.

Reeder, R. J. (1996) Interaction of divalent cobalt, zinc, cadmium, and barium with the calcite surface during layer growth. *Geochim. Cosmochim. Acta* **60**, 1543–1552.

Rihs, S., Condomines, M. and Sigmarsson, O. U. (2000) Ra and Ba incorporation during precipitation of hydrothermal carbonates: Implications for ^{226}Ra–Ba dating of impure travertines. *Geochim. Cosmochim. Acta* **64**, 661–671.

Román-Ross, G., Cuello, G. J., Turrillas, X., Fernández-Martínez, A. and Charlet, L. (2006) Arsenite sorption and co-precipitation with calcite. *Chem. Geol.* **233**, 328–336.

Shahwan, T., Atesin, A. C., Erten, H. N. and Zararsiz, A. (2002) Uptake of Ba^{2+} ions by natural bentonite and $CaCO_3$: A radiotracer, EDXRF and PXRD study. *Journal of Radioanalytical and Nuclear Chemistry* **254**, 563–568.

Shahwan, T., Zünbül, B. and Akar, D. (2005) Study of the Scavenging Behavior and Structural Changes Accompanying the Interaction of Aqueous Pb^{2+} and Sr^{2+} Ions with Calcite. *Geochem. J.* **39**, 317–326.

Stipp, S. L. and Hochella, M. F. (1991) Structure and bonding environments at the calcite surface as observed with X-ray photoelectron spectroscopy (XPS) and low energy electron diffraction (LEED). *Geochim. Cosmochim. Acta* **55**, 1723–1736.

Terakado, Y. and Taniguchi, M. (2006) Method for the study of trace element partitioning between calcium carbonate and aqueous solution: A test case for Sr and Ba incorporation into calcite. *Geochem. J.* **40**, 161–170.

Wang, Y. and Xu, H. (2001) Prediction of trace metal partitioning between minerals and aqueous solutions: a linear free energy correlation approach, *Geochim. Cosmochim. Acta* **65**, 1529–1543.

Xu, N., Hochella, M. F., Jr., Brown, G. E., Jr. and Parks, G. A. (1996) Co(II) sorption at the calcite-water interface: I. X-ray photoelectron spectroscopic study. *Geochim. Cosmochim. Acta* **60**, 2801–2815.

Zhu, C. (2002) Estimation of surface precipitation constants for the sorption of divalent metals onto hydrous ferric oxide and calcite. *Chem. Geol.* **188**, 23–32.